

Atomic-Scale Characterization of Graphene Grown on Copper (100) Single Crystals

Haider I. Rasool,^{†,‡,§,∇} Emil B. Song,^{‡,||,⊥,∇} Matthew Mecklenburg,^{‡,#} B. C. Regan,^{‡,#} Kang L. Wang,^{‡,||} Bruce H. Weiller,^{*,⊥} and James K. Gimzewski^{*,†,‡,§}

[†]Department of Chemistry and Biochemistry, University of California at Los Angeles, Los Angeles, California 90095, United States

[‡]California NanoSystems Institute, University of California at Los Angeles, Los Angeles, California 90095, United States

[§]International Center for Materials Nanoarchitectonics (MANA), 1-1 Namiki, Tsukuba, Ibaraki 305-0044, Japan

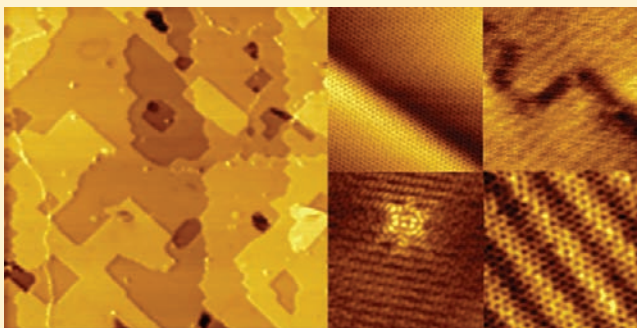
^{||}Department of Electrical Engineering, University of California at Los Angeles, Los Angeles, California 90095, United States

[⊥]Micro/Nano Technology Department, Space Materials Laboratory, The Aerospace Corporation, Los Angeles, California 90009, United States

[#]Department of Physics and Astronomy, University of California at Los Angeles, Los Angeles, California 90095, United States

S Supporting Information

ABSTRACT: Growth of graphene on copper (100) single crystals by chemical vapor deposition has been accomplished. The atomic structure of the graphene overlayer was studied using scanning tunneling microscopy. A detailed analysis of moiré superstructures present in the graphene topography reveals that growth occurs in a variety of orientations over the square atomic lattice of the copper surface. Transmission electron microscopy was used to elucidate the crystallinity of the grown graphene. Pristine, defect-free graphene was observed over copper steps, corners, and screw dislocations. Distinct protrusions, known as “flower” structures, were observed on flat terraces, which are attributed to carbon structures that depart from the characteristic honeycomb lattice. Continuous graphene growth also occurs over copper adatoms and atomic vacancies present at the single-crystal surface. The copper atom mobility within vacancy islands covered with suspended graphene sheets reveals a weak graphene–substrate interaction. The observed continuity and room-temperature vacancy motion indicates that copper mobility likely plays a significant role in the mechanism of sheet extension on copper substrates. Lastly, these results suggest that the quality of graphene grown on copper substrates is ultimately limited by nucleation at the surface of the metal catalyst.



INTRODUCTION

The two-dimensional honeycomb lattice of carbon atoms known as graphene has captured the attention of researchers because of its remarkable electronic^{1,2} and mechanical properties.^{3,4} Initial electronic measurements^{5–7} used pristine graphene sheets isolated by mechanical exfoliation from naturally occurring graphite on unique silicon-insulator substrates.⁸ While devices derived by exfoliation have provided scientists with valuable insights into the electronic transport and mechanics of this remarkable material, a more scalable method for obtaining isolated graphene sheets is required for widespread use. To this end, graphene has been synthesized by physical desorption of Si from SiC single-crystal surfaces,^{9,10} by chemical treatments of graphite,^{11–13} and from small organic molecules involving different metal substrates.^{14–20}

Of particular interest is the growth of graphene on copper substrates,^{18–20} which provides many unique advantages, such as industrial scalability and efficient processing of grown films. In fact, large-scale fabrication of graphene by chemical vapor deposition

(CVD) on copper foils¹⁸ has been used to assemble transparent electrodes and commercial prototype touchscreen displays.²¹ In order to realize further high-quality electronic devices and rational materials from this method of synthesis, atomic-scale characterization of grown graphene and a fundamental understanding of the mechanisms governing the growth process are of great importance. Recent scanning tunneling microscopy (STM)²² and low-energy electron microscopy/low-energy electron diffraction (LEEM/LEED)²³ studies of graphene on polycrystalline copper substrates have revealed that graphene extension can occur on crystal grains that are oriented in such a way that the square atomic lattice of the Cu(100) surface can act as a suitable solid support for catalysis of graphene growth, with the LEEM/LEED studies suggesting that the (100) face is the primary exposed facet. While studies of polycrystalline substrates provide valuable information regarding

Received: January 24, 2011

Published: July 06, 2011

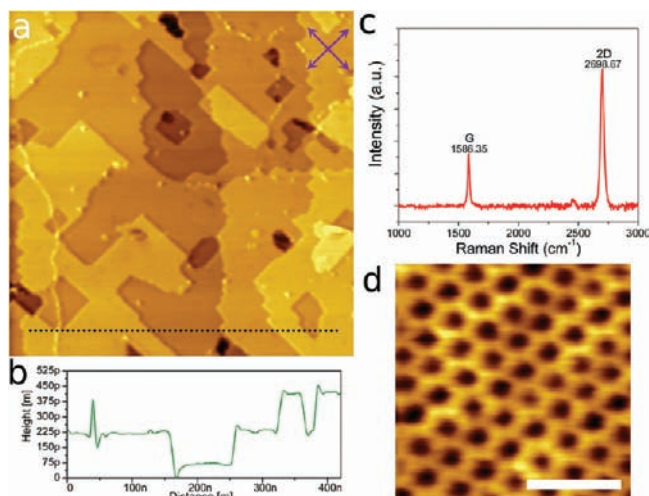


Figure 1. Characterization of as-grown graphene on Cu(100) single crystals. (a) Large-area STM image of sample surface [tunneling current (I_t) = 1.0 nA, sample voltage (V_s) = -75 mV]. Purple arrows act as a compass, indicating the {011} directions of the copper crystal. (b) Line profile recorded along the dotted line in (a), showing single copper atom steps. (c) Typical Raman spectrum of the crystal after growth. (d) Atomic-resolution STM image of the graphene overlayer (I_t = 5.0 nA, V_s = -75 mV, scale bar = 0.75 nm).

growth, characterization and growth on single-crystal substrates allows for a deeper understanding without the presence of surface features such as copper grain boundaries, orientation of identical crystal grains in different directions, and large areas of exposed facets of different identities whose surface arrangement of atoms vary dramatically.

In this article, we show STM topographs of as-grown graphene produced by CVD through the thermal decomposition of methane on high-purity Cu(100) single-crystal substrates at elevated temperatures [see the Supporting Information (SI)]. Observation of the large-scale morphology of samples was accomplished over hundreds of square nanometers with atomic-resolution images acquired at specific features of interest. Raman spectroscopy has revealed that it is possible to grow high-quality graphene on the Cu(100) surface. Through detailed moiré analysis of the superstructures present in atomic-resolution images of the graphene overlayer, the carbon lattice is shown to grow in different orientations with respect to the atomic lattice of the copper crystal. Transmission electron microscopy (TEM) has been used to show that the lack of a clear epitaxial relationship between the graphene honeycomb lattice and the Cu(100) square lattice translates into the growth of polycrystalline graphene islands and continuous sheets. The perfect continuous carbon lattice was observed to exist over copper step edges, corners, and screw dislocations present at the surface, which are generally thought to provide barriers to efficient sheet extension, creating defect structures in the carbon lattice.¹⁴ Distinct protrusions, known as “flower” structures, were observed over the sample surface and are attributed to breaks from the standard hexagonal bonding within the carbon atomic lattice. Grown graphene is also shown to be continuous over small copper adatom clusters and vacancy islands present at the surface of the single crystal. These vacancy islands show significant copper atom mobility at room temperature beneath suspended graphene sheets. Lastly, we discuss the implications of these observations

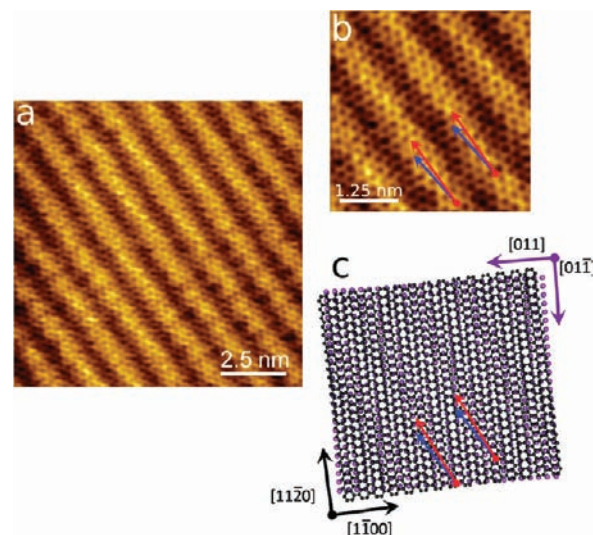


Figure 2. Moiré structure of graphene at a 3.5° angle with respect to the underlying copper crystal. (a) Large-area image illustrating the linear periodic modulation of the graphene overlayer. (b) High-resolution image of the graphene structure. The parallel red arrows, which have a spacing of 1.25 nm and indicate the direction of the moiré pattern, make a 10° angle with the [1100] graphene direction, which is highlighted with blue arrows. (c) Hard-sphere atomic model of the two lattices. The black arrows and lattice belong to graphene, and the purple arrows and spheres belong to the copper substrate. Imaging parameters in (a) and (b): I_t = 1.45 nA, V_s = -75 mV.

in the context of the mechanism of graphene growth on copper substrates.

RESULTS AND DISCUSSION

Large-scale STM images of Cu(100) single-crystal surfaces overgrown with graphene (Figure 1a) at full surface coverage show large, atomically flat terraces that have surface areas of a few hundred square nanometers. The total height variation over 500 nm² was only 1.98 nm, which is more than an order of magnitude lower than what has been observed for similar areas of graphene grown on polycrystalline copper substrates.²² Each atomically flat terrace has step edges that come together in right-angle corners that are aligned along the {011} crystal directions with step heights of ~0.18 nm, which is characteristic of the Cu(100) surface (see the SI). In order to highlight the small height variation over the copper surface, a cross section of Figure 1a is provided in Figure 1b. In this line profile, three distinct levels of copper terraces with atomic flats that proceed for more than 100 nm can be clearly observed. These large terraces, which are present throughout the sample, have smaller scattered rectangular islands and pits with single monatomic step heights that are overgrown with defect-free graphene.

In addition to acquiring STM topographs, we characterized the graphene overlayer using Raman spectroscopy. Figure 1c shows a typical Raman spectrum of as-grown graphene on a single crystal after subtraction of the copper luminescent background. The peak located at ~2700 cm⁻¹ (the 2D band) is symmetric with a full width at half-maximum (fwhm) of 33 cm⁻¹ and is more than twice as intense as the peak located at ~1600 cm⁻¹ (the G band). No measurable peak was observed at ~1350 cm⁻¹ (the D band). These results are consistent with the synthesis of high-quality monolayer graphene.^{24,25}

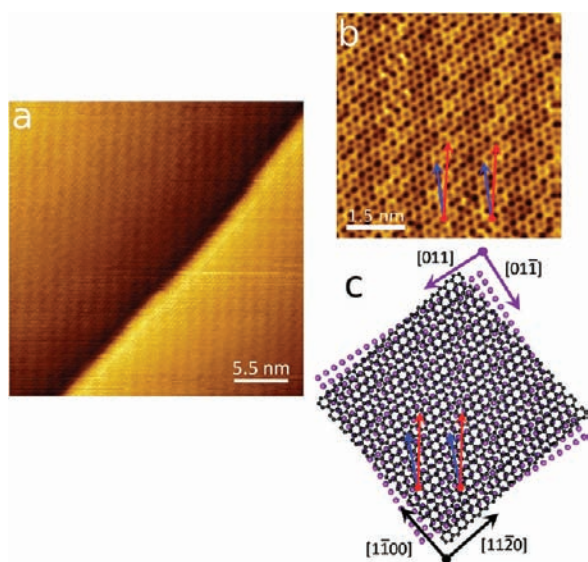


Figure 3. Moiré structure of graphene at a 10.0° angle with respect to the underlying copper crystal. (a) Large-area image illustrating the linear periodic modulation of the graphene overlayer. (b) High-resolution image of the graphene structure. The parallel red arrows, which have a spacing of 1.35 nm and indicate the direction of the moiré pattern, make an 8.5° angle with the $[11\bar{2}0]$ graphene direction, which is highlighted with blue arrows. (c) Hard-sphere atomic model of the two lattices. The black arrows and lattice belong to graphene, and the purple arrows and spheres belong to the copper substrate. Imaging parameters in (a) and (b): $I_t = 5.50$ nA, $V_s = -75$ mV.

Once large-area images of the surface had been obtained, we characterized the atomic structure of the graphene overlayer (Figure 1d) and its registry with the copper lattice. This was accomplished by analyzing higher-order periodic modulations in atomic-resolution images of the graphene overlayer. These modulations are attributed to the convolution of the electronic structure of the square lattice of the copper crystal and the carbon honeycomb lattice of graphene, which interact to produce unique moiré superstructures in STM topographs.^{15,17}

Atomic-resolution images taken at different areas of the single-crystal surface show a variety of moiré superstructures, indicating that graphene grows in different orientations with respect to the underlying lattice. In certain STM images acquired over flat terraces of the surface, the graphene overlayer has a moiré superstructure with a well-defined linear periodic modulation, as shown in Figure 2a,b. These alternating bands in the STM topographs have a 1.25 nm spatial modulation frequency and make an angle of 10° with the $[1\bar{1}00]$ direction of the graphene sheet. On the basis of the known directions of the Cu(100) single-crystal surface and moiré pattern simulations, the linear superstructure is attributed to the case where the graphene $[11\bar{2}0]$ direction makes a small angle of 3.5° with the $[01\bar{1}]$ direction of the copper. The result of a moiré simulation of this structure is provided as the hard-sphere model shown in Figure 2c. One of the larger angular differences found between the graphene sheet and the copper lattice produces the moiré pattern shown in Figure 3a,b. In these areas, alternating bright and dark regions again can be observed, with a different overall moiré pattern. These linear bands make an angle of 8.5° with the indicated $[11\bar{2}0]$ direction of the graphene layer and have a slightly larger spatial modulation frequency of 1.35 nm. This

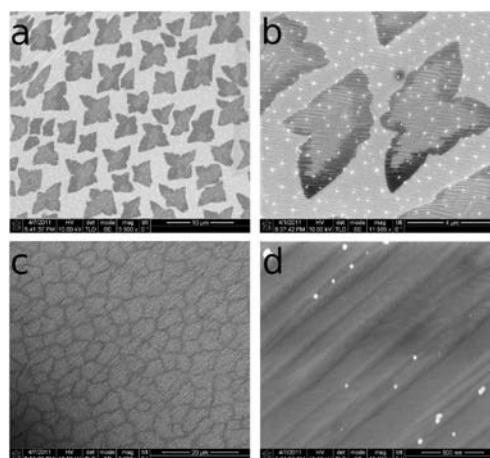


Figure 4. SEM images of graphene growth on Cu(100) single crystals. (a) Large-area and (b) high-magnification images of partial surface coverage, illustrating the typical four-lobed geometry of individual islands. (c) Large-area and (d) high-magnification images of graphene growth after full surface coverage.

observed STM topography is attributed to the case where the graphene $[11\bar{2}0]$ direction makes a 10° angle with the $[01\bar{1}]$ direction of the copper. The result of the moiré simulation of this larger angular orientation is shown in Figure 3c.

The observation of multiple orientations of the graphene layer with respect to the copper crystal has important implications regarding the CVD growth. First, graphene does not have a clear preferred orientation, which is likely the result of a weak interaction between the copper lattice and the extending graphene sheet. Second, the grain boundaries that form between two different nucleated graphene sheets that bond together contain carbon structures other than the ideal hexagonal carbon lattice to accommodate lattice mismatches. These grain boundaries can dramatically alter the electron transport^{26,27} and provide potential sites for mechanical failure under an applied stress.²⁸ Without the ability of the underlying substrate to minimize the mismatch between sheets, careful control of the nucleation rate on copper surfaces is necessary in order to synthesize large areas of high-quality graphene. Additionally, a variety of surface adsorption measurements can be accomplished on a single sample to study possibilities of opening a band gap in post-modified graphene, as has been previously reported for growth on Ir(111) crystals.²⁹

With the observation of multiple orientations of the graphene overlayer with respect to the copper lattice, we sought to characterize the growth evolution and crystallinity of the resulting graphene film using scanning electron microscopy (SEM) and TEM. Using SEM, we visualized the growth at partial and full surface coverage. Figure 4a,b shows typical SEM images of the partial growth of graphene islands on the crystal surface. The islands have a characteristic four-lobed structure, which has been reported previously for graphene growth on polycrystalline foils.^{18,23} One possible explanation of the observed island shape can be attributed to the fourfold symmetry of the underlying copper lattice rather than the sixfold symmetry of the graphene hexagonal lattice. Mobile carbon atoms at the surface, or carbon-carrying copper atoms, are expected to diffuse along one of the four equivalent lattice axes of the copper substrate before extending the growing island along one of the surface directions.

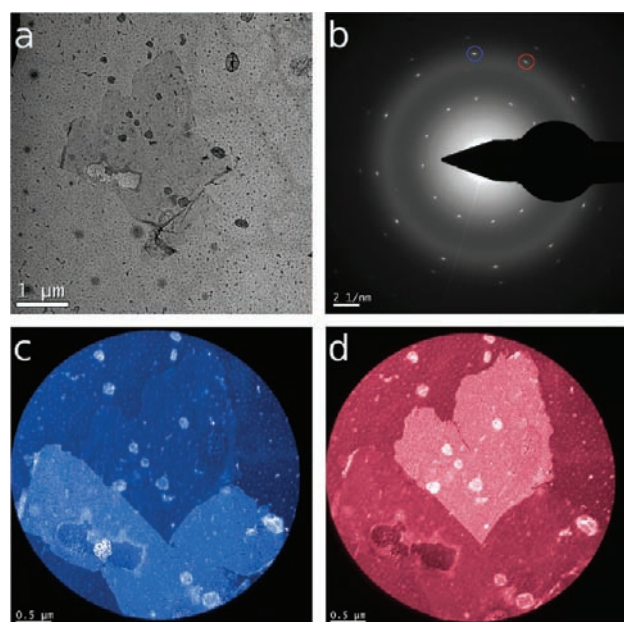


Figure 5. TEM analysis of a graphene island. (a) Bright-field image of a transferred island supported on a TEM window. (b) SAED pattern of the illuminated island in (a), illustrating two distinct crystallographic orientations of graphene within the island. (c) DF-TEM image showing the real-space distribution of the crystal orientation when the objective aperture was placed over the diffraction spot circled in blue in (b). (d) DF-TEM image showing the real-space distribution of the second graphene crystal orientation when the objective aperture was placed over the diffraction spot circled in red in (b).

As the reaction proceeds, the entire surface becomes covered with a continuous graphene overlayer. SEM images of the full growth over the entirety of the surface are shown in Figure 4c,d. The apparent grains, or domains, appearing in Figure 4c are attributed to the coalescence of the four-lobed islands into a continuous graphene overlayer.

One natural question that arises from the observed SEM images is whether each isolated island consists of single or multiple orientations of graphene honeycomb lattice. In order to address this issue, we transferred the grown graphene islands to custom-designed TEM windows for imaging and diffraction analysis using a spin-coated polymer support and wet chemical etching of single crystals. The transferred graphene islands showed minimal distortion or wrinkling on the new substrate, as checked by SEM imaging (see the SI). Figure 5a shows a bright-field image of a graphene island on a TEM window. A selected-area electron diffraction (SAED) pattern collected over the graphene island is shown in Figure 5b and reveals two distinct sets of graphene orientations (see the SI for the SAED pattern of a single grain). Measuring the angle between the selected diffraction peaks revealed a 28° rotation between these two sets of lattices. The real-space distribution of the two orientations within the island can be visualized using dark-field TEM (DF-TEM) imaging by collecting specific diffracted electrons through an objective aperture placed in the back focal plane of the objective lens.³⁰ Figure 5c,d shows the DF-TEM images generated when diffracted electrons were collected from the circled regions shown in red and blue in Figure 5b. From the DF-TEM image, it is clear that the upper lobe of the island consists of one crystalline domain and the rest of the island belongs to another domain having a different orientation.

In view of the polycrystallinity of the graphene islands, it is expected that as the graphene grows over the entirety of the surface, the resulting continuous layer will contain many domains of different orientations as well. To corroborate this assertion, continuous graphene samples from fully covered single crystals were also transferred to TEM windows and analyzed. A bright-field image of a continuous graphene sheet and the SAED pattern of the same area are shown in Figure 6a,e. From the SAED pattern, it is clear that there are three distinct graphene orientations present in the illuminated area, corresponding to the blue, yellow, and red circles in Figure 6e. Measuring the angles of the diffraction peaks, we found that the blue domain is oriented at an angle of 28° relative to the yellow domain, which in turn is oriented at an angle of 4° relative to the red domain. Selecting each of the distinct diffraction spots and imaging using DF-TEM, again, allowed for the real-space visualization of the distribution of the different graphene orientations. The highlighted areas in Figure 6b–d show that the illuminated area has three distinct grains that have come together to form a continuous juncture within the grown graphene overlayer.

In order to grow high-quality graphene on copper, it is also important to understand which surface features in the copper contribute to defects in the growing carbon atomic lattice. In growth models where the catalytic surface is treated as a stagnant structure, breaks in flat terraces at monatomic step edges and corners of the metal surface present possible sites for defect formation. Hence, these surface features are actively being studied both theoretically and experimentally.^{31,32} In an upward growth over a monatomic copper step or corner, the extending carbon front of the graphene sheet may terminate through bonding of the carbon σ bonds to adjacent copper atoms of the overlayer. During growth in the downward direction, the carbon σ bonds are uninhibited by the copper substrate, and continuous growth is expected.

In our experiments, continuous growth of graphene in a “carpet” draping over monatomic steps and corners was consistently observed on the Cu(100) surface (Figure 7a). Figure 7b shows a current image acquired simultaneously with the image presented in Figure 7a. It clearly highlights the continuity of the overlayer, since a large disparity exists between the small vertical corrugations of the graphene atomic lattice and the larger atomic step heights of copper. From Figure 7a,b, it is clear that graphene not only spans the edges of the steps but also grows continuously over the two different types of corners, which are characterized by either seven surrounding copper atoms (turquoise sphere in Figure 7c) or three surrounding atoms (green sphere in Figure 7c). This uninhibited growth over the copper surface may be the result of high copper adatom and island mobility at the growth temperatures of 1000°C , where carbon-carrying copper atoms can extend the sheet front in a type of “tiling” over the various surface structures.²² In order to accomplish growth up or down steps, the nearly fully coordinated corners present during growth (turquoise sphere in Figure 7c) provide high-probability sites for atomic diffusion across steps, since diffusing atoms follow trajectories that maximize coordination during motion.³³ The corners with lower coordination (green sphere in Figure 7c) have higher barriers for diffusion across the step boundaries and provide open sites for possible interactions with an extending graphene sheet. Surprisingly, continuous growth over edges and both types of corners of the various smaller rectangular pits and islands present on the sample surface was

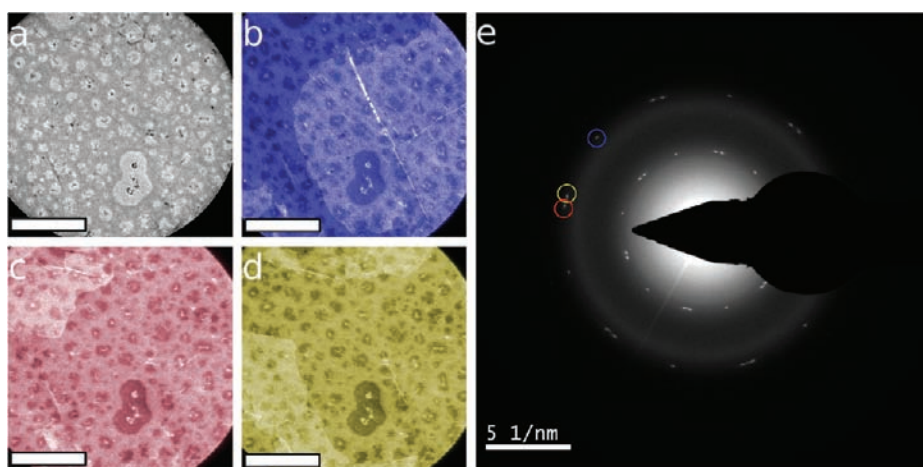


Figure 6. TEM analysis of full graphene growth. (a) Bright-field image of a transferred graphene sheet supported on a TEM window. (b–d) DF-TEM images showing the real-space distribution of different crystal orientations within the continuous graphene sheet when the objective aperture was placed over different diffraction spots of the illuminated region. Scale bars for (a–d) represent 1 μm . (e) SAED pattern acquired over the illuminated region shown in (a), revealing the presence of three distinct crystallographic orientations of graphene. Colored circles show the positions of the objective aperture when the DF-TEM images in (b–d) were acquired.

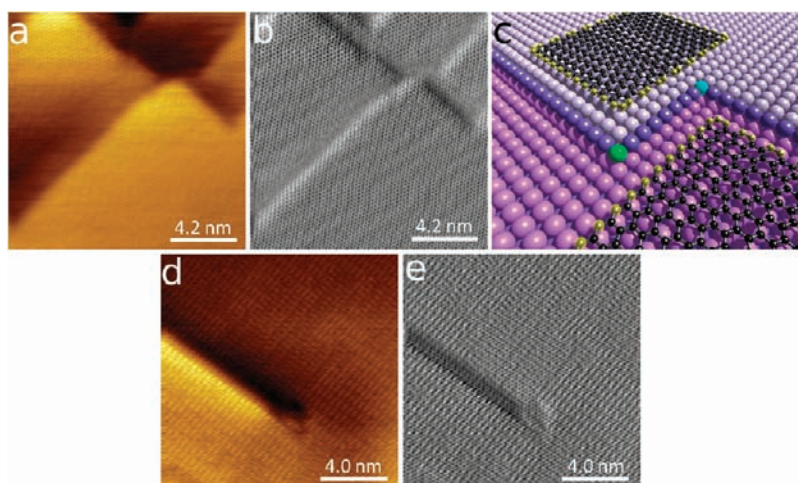


Figure 7. Atomic-resolution images of continuous defect-free growth of graphene over Cu(100) single crystals. (a) STM topograph and (b) simultaneously acquired current image of graphene growth over copper monatomic step edges and corners. (c) Illustration of graphene growth over steps and corners of the Cu(100) single-crystal surface. Magenta spheres belong to the lower terrace, gray spheres to the upper terrace, and dark-purple spheres to the copper step edges. Two different types of copper corner atoms are colored in green and turquoise. Frontier carbon atoms are highlighted in yellow. (d) STM topograph and (e) corresponding current image of defect-free growth over a screw dislocation in the copper substrate. Imaging parameters: (a, b) $I_t = 1.74 \text{ nA}$, $V_s = -75 \text{ mV}$; (d, e) $I_t = 5.50 \text{ nA}$, $V_s = -75 \text{ mV}$.

observed, revealing uninhibited growth in both the upward and downward directions.

Continuous graphene growth over dislocations on the copper surface was also observed. Figure 7d,e shows graphene growth over a screw dislocation present on the copper surface. This screw dislocation is formed from the propagation of a double step edge out of a single terrace of atoms in the copper. While the screw dislocation may move laterally across the surface during growth, the structural identity is expected to remain constant, providing a unique surface topography for graphene sheet extension.

When the graphene overlayer was imaged, a variety of protrusions and depressions were found over the sample surface. One interesting type of protrusion is a “flower” structure. This type of structure was observed previously on SiC-grown graphene and is attributed to a defect that perturbs the electronic

structure of graphene.^{26,34–36} A pair of these defects is shown in Figure 8a, and a different isolated flower structure is shown in Figure 8b. These structures do not appear to show any correlation with specific surface features present in the copper single crystal. The exact nature and atomic origin of this unique structure is currently under investigation, since the presence of scattering centers and possible breaks in the perfect honeycomb lattice are expected to have profound effects on the electronic and mechanical properties of the grown graphene.^{26–28} For instance, defect engineering of graphene sheets can produce localized one-dimensional metallic states within the carbon lattice³⁷ for use in electronics applications.

Observation of this type of defect on a substrate other than SiC-grown graphene suggests that the scattering source is independent of the identity of the underlying material and likely

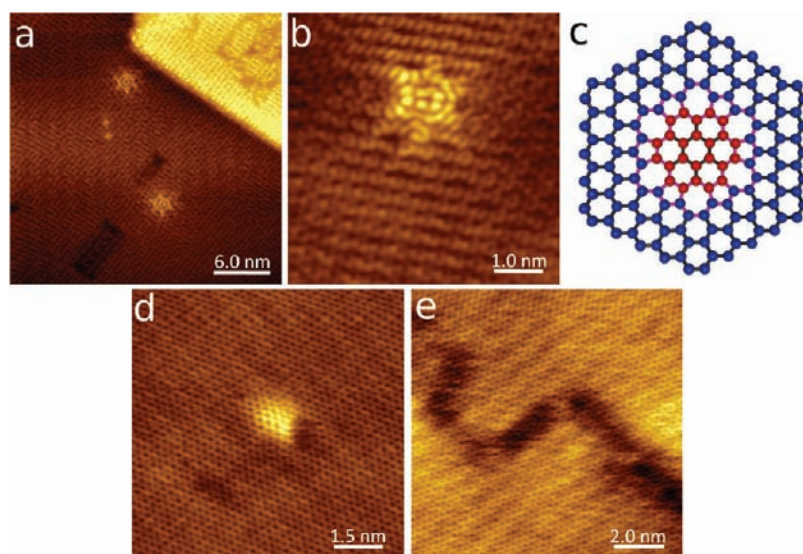


Figure 8. Small protrusions and depressions present on the sample surface. (a) STM image of two “flower” structures and two rectangular depressions. (b) High-resolution STM image of a flower structure in the carbon atomic lattice of graphene. (c) Atomic model of the flower structure proposed in ref 36. Red spheres belong to an “inner” piece of graphene that is rotated by 30° with respect to the rest of the graphene sheet (the “outer” portion), which is represented by blue spheres. The two domains are stitched together by six pentagon–heptagon pairs, as highlighted by the magenta bonds in the model. (d) Continuous graphene growth over a copper adatom of the single crystal. (e) Pristine graphene suspended over atomic vacancies of the Cu(100) square lattice. Imaging parameters: (a) $I_t = 5.50$ nA, $V_s = -75$ mV; (b) $I_t = 1.75$ nA, $V_s = -75$ mV; (d) $I_t = 1.40$ nA, $V_s = -75$ mV; (e) $I_t = 1.74$ nA, $V_s = -75$ mV.

due to a structure formed within the carbon atomic lattice. A survey of current experimental and theoretical STM work on defect structures and their appearance in STM topographs was performed in an attempt to identify the origin of this structure.^{38,39} Recent results on SiC suggest that the flower structure results from a rotational defect wherein a symmetric core of seven connected hexagons is rotated by 30° (or equivalently 90°) with respect to the remaining graphene lattice and stitched into the sheet with a closed loop of five- and seven-membered rings.³⁶ A recent high-resolution TEM analysis of CVD-grown graphene has shown experimentally that this proposed structure does exist.⁴⁰ A ball-and-stick model of the structure proposed in ref 36 is provided in Figure 8c, where the center of the red group of carbon atoms corresponds to the centers of the “flowers” observed in the STM images. The density functional theory calculations performed in that work showed good agreement with the experimental STM topography and accurately predicted the observed height profile of the structures found in the graphene grown on Cu(100) single-crystals in this work. An interesting observation supporting the assertion that the defect originates from a structure present within the graphene lattice is that the orientation and symmetry of the two defects present in Figure 8a are identical with each of the six “petals” positioned along the six directions of the carbon atomic lattice. This was also seen in STM images in previous reports of SiC-grown graphene.³⁴

In addition to the above-mentioned carbon structure, it was possible to observe graphene growth over defects within the underlying copper single crystal. Figure 8d shows growth over a protrusion in the substrate that is attributed to a small cluster of copper adatoms with a height that corresponds to a single monatomic copper step. There is no break in the carbon atomic lattice and no change in orientation of the moiré pattern present on the atomically flat terraces, nor are any scattering waves present near the protrusion, indicating minimal perturbation of the structure of the sheet. Figure 8e shows a typical atomic-resolution

image of an observed depression present in one of the atomically flat terraces of the sample. Under normal imaging conditions, these small regions have a height that is typically 30–60 pm lower than the surrounding terrace. The pristine atomic structure of the graphene sheet spans the depressed region where the moiré pattern is absent. Additionally, these depressed regions often have the same square symmetry of the underlying atomic lattice, as can be seen in Figure 8e and the dark rectangular regions present in Figure 8a. From these observations, we conclude that the depressions are copper atom vacancies in the flat terraces of the crystal covered with a continuous suspended sheet of graphene.

Interestingly, the depressions discussed above are not always static structures on the surface and often span large areas of tens of square nanometers (see the SI). Figure 9 shows a series of images taken over an area of 20 nm^2 where two of these “moiré defects” show significant mobility at room temperature. Each image was taken over the same scan area, under identical scan parameters, with the static kink in the terrace edge serving as a reference point for observation of the copper motion. In order to explain the changes in the shape of the vacancies, four distinct types of copper atom diffusion events may be considered: (1) arrival of a copper atom at an edge or corner, (2) diffusion along the edge of the vacancy, (3) movement across a corner where two edges meet, and (4) dissociation from a vacancy edge or corner into the vacancy. In the absence of the suspended graphene sheet, each of these distinct types of motion is expected to result in an increase in energy since diffusing copper atoms prefer to decrease their overall coordination number during mobility.³³ Evidence for each of the diffusion events can be seen in Figure 9, with nucleation and dissociation of a small copper island within the vacancy shown in Figure 9g.

The observed mobility within the vacancies reveals that carbon atoms of the suspended sheet do not interact strongly with the copper substrate, since a strong interaction would be

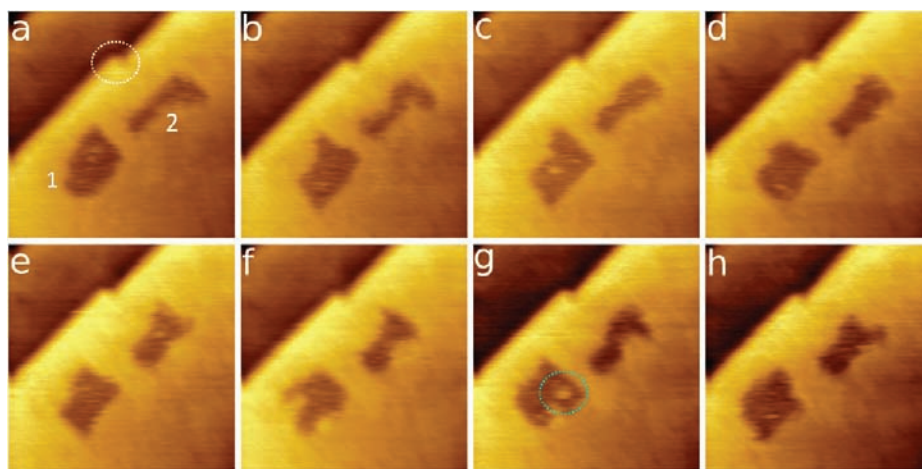


Figure 9. Copper atom mobility within vacancy islands covered with a continuous suspended sheet of graphene. The white circle highlights a static kink present on the terrace edge that serves as a reference for visualizing the copper motion. The green circle highlights the formation and dissolution of a small copper atom cluster within the vacancy. Each of the 20 nm² images was acquired in 115 s with $I_t = 1.00$ nA and $V_s = -100$ mV.

expected to pin the copper edges and trapped atoms of the vacancy, resulting in static structures in the STM topographs. While quantitative estimations of the strength of the interaction between the suspended sheet and the underlying copper surface are beyond the scope of the current work, it is interesting to note that over larger vacancies it is possible to lift the central areas of the suspended graphene sheet by altering the interaction between the STM tip and the graphene sheet. This is similar to what has been shown for exfoliated graphene on SiO₂ substrates.⁴¹ Near the edges of the vacancies, the graphene appears depressed, whereas the central region of these vacancies can undergo reversible deformation depending on the imaging parameters (see the SI). These observations suggest that the strength of the interaction between the graphene sheet and the copper may be close to that of a weak van der Waals-type interaction rather than a more pronounced interaction resulting from significant overlap of the carbon p_z and copper d orbitals.

The mobility of copper atoms beneath the suspended graphene imaged at room temperature suggests that copper atom diffusion may also play an important role in the extension of the carbon lattice during growth. These mobile copper atoms may act as carbon carriers and efficiently extend the growing sheet over the steps and different corners present on the surface of copper substrates.²² While the weak interaction between the carbon and copper atoms permits significant surface diffusion, it also allows for the formation of a variety of relative orientations of the two lattices, creating potential mismatches between neighboring graphene domains. Recent work has shown that to minimize the formation of scattering sources and generate large crystalline domains, altering growth parameters such as flow rate, temperature, chamber pressure, and local growth environment can have substantial effects on the size of graphene crystallites, which are ultimately determined by the average spacing of nucleation sites on the copper surface.^{42,43}

CONCLUSIONS

In conclusion, the atomic-scale characterization of graphene grown on Cu(100) single crystals by thermal decomposition of methane has been accomplished using STM. Graphene has been found to grow over the square lattice of Cu(100) single crystals in a variety of orientations, which is expected to produce grain

boundaries that contain carbon structures that depart from the ideal honeycomb lattice of graphene.³⁰ Through TEM characterization of graphene grown at partial and full surface coverage of single crystals, it has been shown that the varied orientations give rise to nucleated islands and continuous graphene films that are polycrystalline in nature. The observed growth over steps, corners, and screw dislocations and the room-temperature mobility of the underlying copper atoms suggest that substrate motion may play a significant role in the growth mechanism of graphene sheet extension on copper substrates. The observed variation in the graphene growth orientation, in combination with the continuity over the various surface features of the Cu(100) single crystals, has revealed that the quality of the grown graphene is ultimately limited by the nucleation at the surface rather than the exact nature of the atomic structure of the underlying copper substrate. A fundamental understanding of the growth mechanism will help elucidate the factors that contribute to formation of the “flower” structures observed within the graphene lattice grown on copper crystals and may allow researchers to grow wafer-scale pristine graphene sheets. Future mechanistic studies may also aid in the rational incorporation of dopant atoms, such as nitrogen and boron, for electronic device applications.

ASSOCIATED CONTENT

S Supporting Information. Materials and methods, hard-sphere illustrations of the Cu(100) and graphene atomic lattices, SEM images of partial growth on copper and after transfer, small-area bright-field TEM image of graphene and SAED pattern of a single graphene domain, STM image of a large-area copper vacancy overgrown with graphene, reversible deformation of suspended graphene sheets, and complete refs 21 and 29. This material is available free of charge via the Internet at <http://pubs.acs.org>.

AUTHOR INFORMATION

Corresponding Author

gimzewski@cnsi.ucla.edu; bruce.h.weiller@aero.org

Author Contributions

∇ These authors contributed equally.

ACKNOWLEDGMENT

H.I.R. and J.K.G. thank the MEXT WPI Program: International Center for Materials Nanoarchitectonics (MANA) of Japan for financial support. E.B.S. and K.L.W. thank the Functional Engineered NanoArchitectonics (FENA) Center at UCLA for financial support. E.B.S. acknowledges financial support from the NSF IGERT Materials Creation Training Program (Grant DGE-11443). B.H.W. acknowledges support from The Aerospace Corporation's Independent Research and Development Program. E.B.S. thanks J. D. Fowler for invaluable help with the CVD apparatus at The Aerospace Corporation. All TEM work was performed at the Electron Imaging Center for NanoMachines in the CNSI at UCLA. E. R. White is acknowledged for help with TEM sample preparation. H.I.R. thanks H. D. Tran for fruitful discussions and K. A. Lopata for help with the moiré analysis of STM images and helpful discussions.

REFERENCES

- Geim, A. K.; Novoselov, K. S. *Nat. Mater.* **2007**, *6*, 183.
- Castro Neto, A. H.; Guinea, F.; Peres, N. M. R.; Novoselov, K. S.; Geim, A. K. *Rev. Mod. Phys.* **2009**, *81*, 109.
- Lee, C.; Wei, X.; Kysar, J. W.; Hone, J. *Science* **2008**, *321*, 385.
- Bunch, J. S.; van der Zande, A. M.; Verbridge, S. S.; Frank, I. W.; Tanenbaum, D. M.; Parpia, J. M.; Craighead, H. G.; McEuen, P. L. *Science* **2007**, *315*, 490.
- Novoselov, K. S.; Geim, A. K.; Morozov, S. V.; Jiang, D.; Zhang, Y.; Dubonos, S. V.; Grigorieva, I. V.; Firsov, A. A. *Science* **2004**, *306*, 666.
- Novoselov, K. S.; Geim, A. K.; Morozov, S. V.; Jiang, D.; Katsnelson, M. I.; Grigorieva, I. V.; Dubonos, S. V.; Firsov, A. A. *Nature* **2005**, *438*, 197.
- Zhang, Y.; Tan, Y.-W.; Stormer, H. L.; Kim, P. *Nature* **2005**, *438*, 201.
- Novoselov, K. S.; Jiang, D.; Schedin, F.; Booth, T. J.; Khotkevich, V. V.; Morozov, S. V.; Geim, A. K. *Proc. Natl. Acad. Sci. U.S.A.* **2005**, *102*, 10451.
- Berger, C.; Song, Z.; Li, X.; Wu, X.; Brown, N.; Naud, C.; Mayou, D.; Li, T.; Hass, J.; Marchenkov, A. N.; Conrad, E. H.; First, P. N.; de Heer, W. A. *Science* **2006**, *312*, 1191.
- Emtsev, K. V.; Bostwick, A.; Horn, K.; Jobst, J.; Kellogg, G. L.; Ley, L.; McChesney, J. L.; Ohta, T.; Reshanov, S. A.; Röhrl, J.; Rotenberg, E.; Schmid, A. K.; Waldmann, D.; Weber, H. B.; Seyller, T. *Nat. Mater.* **2009**, *8*, 203.
- Gilje, S.; Han, S.; Wang, M.; Wang, K. L.; Kaner, R. B. *Nano Lett.* **2007**, *7*, 3394.
- Tung, V. C.; Allen, M. J.; Yang, Y.; Kaner, R. B. *Nat. Nanotechnol.* **2009**, *4*, 25.
- Park, S.; Ruoff, R. S. *Nat. Nanotechnol.* **2009**, *4*, 217.
- Sutter, P. W.; Flege, J.-I.; Sutter, E. A. *Nat. Mater.* **2008**, *7*, 406.
- Coraux, J.; N'Diaye, A. T.; Busse, C.; Michely, T. *Nano Lett.* **2008**, *8*, 565.
- Reina, A.; Jia, X.; Ho, J.; Nezhich, D.; Son, H.; Bulovic, V.; Dresselhaus, M. S.; Kong, J. *Nano Lett.* **2009**, *9*, 30.
- Ueta, H.; Saida, M.; Nakai, C.; Yamada, Y.; Sasaki, M.; Yamamoto, S. *Surf. Sci.* **2004**, *560*, 183.
- Li, X.; Cai, W.; An, J.; Kim, S.; Nah, J.; Yang, D.; Piner, R.; Velamakanni, A.; Jung, L.; Tutuc, E.; Banerjee, S. K.; Colombo, L.; Ruoff, R. S. *Science* **2009**, *324*, 1312.
- Gao, L.; Guest, J. R.; Guisinger, N. P. *Nano Lett.* **2010**, *10*, 3512.
- Zhao, L.; Rim, K. T.; Zhou, H.; He, R.; Heinz, T. F.; Pinczuk, A.; Flynn, G. W.; Pasupathy, A. N. 2010, arXiv:cond-mat/1008.3542. arXiv.org e-Print archive. <http://arxiv.org/abs/1008.3542> (accessed Jan 24, 2011).
- Bae, S.; et al. *Nat. Nanotechnol.* **2010**, *5*, 574.
- Rasool, H. I.; Song, E. B.; Allen, M. J.; Wassei, J. K.; Kaner, R. B.; Wang, K. L.; Weiller, B. H.; Gimzewski, J. K. *Nano Lett.* **2011**, *11*, 251.
- Wofford, J. M.; Nie, S.; McCarty, K. F.; Bartelt, N. C.; Dubon, O. D. *Nano Lett.* **2010**, *10*, 4890.
- Ferrari, A. C.; Meyer, J. C.; Scardaci, V.; Casiraghi, C.; Lazzeri, M.; Mauri, F.; Piscanec, S.; Jiang, D.; Novoselov, K. S.; Roth, S.; Geim, A. K. *Phys. Rev. Lett.* **2006**, *97*, No. 187401.
- Graf, D.; Molitor, F.; Ensslin, K.; Stampfer, C.; Jungen, A.; Hierold, C.; Wirtz, L. *Nano Lett.* **2007**, *7*, 238.
- Rutter, G. M.; Crain, J. N.; Guisinger, N. P.; Li, T.; First, P. N.; Stroschio, J. A. *Science* **2007**, *317*, 219.
- Yazyev, O. V.; Louie, S. G. *Nat. Mater.* **2010**, *9*, 806.
- Grantab, R.; Shenoy, V. B.; Ruoff, R. S. *Science* **2010**, *330*, 946.
- Balog, R.; et al. *Nat. Mater.* **2010**, *9*, 315.
- Huang, P. Y.; Ruiz-Vargas, C. S.; van der Zande, A. M.; Whitney, W. S.; Levendorf, M. P.; Kevek, J. W.; Garg, S.; Alden, J. S.; Hustedt, C. J.; Zhu, Y.; Park, J.; McEuen, P. L.; Muller, D. A. *Nature* **2011**, *469*, 389.
- Chen, H.; Zhu, W.; Zhang, Z. *Phys. Rev. Lett.* **2010**, *104*, No. 186101.
- Starodub, E.; Maier, S.; Stass, I.; Bartlet, N. C.; Feibelman, P. J.; Salmeron, M.; McCarty, K. F. *Phys. Rev. B* **2009**, *80*, No. 235422.
- Zhang, Z.; Lagally, M. G. *Science* **1997**, *276*, 377.
- Guisinger, N. P.; Rutter, G. M.; Crain, J. N.; Heiliger, C.; First, P. N.; Stroschio, J. A. *J. Vac. Sci. Technol., A* **2008**, *26*, 932.
- Simon, L.; Bena, C.; Vonau, F.; Aubel, D.; Nasrallah, H.; Habar, M.; Peruchetti, J. C. *Eur. Phys. J. B* **2009**, *69*, 351.
- Cockayne, E.; Rutter, G. M.; Guisinger, N. P.; Crain, J. N.; Stroschio, J. A.; First, P. N. 2010, arXiv:cond-mat/1008.3574. arXiv.org e-Print archive. <http://arxiv.org/abs/1008.3574> (accessed Jan 24, 2011).
- Lahiri, J.; Lin, Y.; Bozkurt, P.; Olyenik, I. I.; Batzil, M. *Nat. Nanotechnol.* **2010**, *5*, 326.
- Yazyev, O. V.; Louie, S. G. *Phys. Rev. B* **2010**, *81*, No. 195420.
- Amara, H.; Latil, S.; Meunier, V.; Lambin, Ph.; Charlier, J.-C. *Phys. Rev. B* **2007**, *76*, No. 115423.
- Meyer, J. C.; Kurasch, S.; Park, H. J.; Skakalova, V.; Künzel, D.; Gross, A.; Chuvilin, A.; Algara-Siller, G.; Roth, S.; Iwasaki, T.; Starke, U.; Smet, J. H.; Kaiser, U. *Nat. Mater.* **2011**, *10*, 209.
- Mashoff, T.; Pratzler, M.; Geringer, V.; Echtermeyer, T. J.; Lemme, M. C.; Liebmann, M.; Morgenstern, M. *Nano Lett.* **2010**, *10*, 461.
- Li, X.; Magnuson, C. W.; Venugopal, A.; An, J.; Won Suk, J.; Han, B.; Borysiak, M.; Cai, W.; Velamakanni, A.; Zhu, Y.; Fu, L.; Vogel, E. M.; Voelkl, E.; Colombo, L.; Ruoff, R. S. *Nano Lett.* **2010**, *10*, 4328.
- Li, X.; Magnuson, C. W.; Venugopal, A.; Tromp, R. M.; Hannon, J. B.; Vogel, E. M.; Colombo, L.; Ruoff, R. S. *J. Am. Chem. Soc.* **2011**, *9*, 2816.